Discrete numerical analysis of drained cyclic loading on a model sand

Alice Ezzeddine, Bogdan Cazacliu, Patrick Richard, Luc Thorel, Riccardo Artoni

Proceedings 10th NUMGE 2023
10th European Conference on Numerical Methods in Geotechnical Engineering
Zdravkovic L, Kontoe S, Taborda DMG, Tsiampousi A (eds)

https://doi.org/10.53243/NUMGE2023-218

Discrete numerical analysis of drained cyclic loading on a model sand

A. Ezzeddine[1], B. Cazacliu[1], P. Richard[1], L. Thorel[2], R. Artoni[1]

[1]*Univ Gustave Eiffel, MAST-GPEM, F-44344 Bouguenais, France*
[2]*Univ Gustave Eiffel, GERS-CG, F-44344 Bouguenais, France*

ABSTRACT: Discrete element method (DEM) is adopted in this work to characterize the behaviour of Fontainebleau sand NE34 under cyclic stress. For that YADE, an open-source software, is used where a linear contact model is utilized. The effect of anisotropic particle shape is modelled by a rolling resistance moment. The model parameters are first calibrated to reproduce experimental data from drained monotonic triaxial tests on NE34. Then, a series of drained cyclic triaxial tests is carried out on an elementary volume sample in homogeneous conditions where the cyclic stress ratio and the density index I_D of the sample vary between different tests. The small strains properties, shear modulus G and damping ratio D, are then evaluated and compared with experimental data from the literature. The accumulation of irreversible deformations is also characterized. Finally, a micro-mechanical analysis of fabric evolution and force transmission allows to link the observed macroscopic behaviour to phenomena at the grain scale, depending on the stress level and I_D initially set.

Keywords: Cyclic drained triaxial tests; DEM simulations; Fontainebleau sand NE34; micro-mechanical analysis

1 INTRODUCTION

Geotechnical structures undergo various types of loadings during their lifespan, such as cyclic loading that can display severe and irreversible effects on the serviceability of structures. The resultant influence of cyclic loading is a function of the magnitude, the number of cycles, and the frequency of application as well as the characteristics of the structure, (Di Prisco and Wood, 2012).

These forms of loadings could originate from various sources such as waves on offshore structures, traffic on roads, construction processes like vibro-installation of piles, and mechanical compaction which all contribute to imposing cycles of loading on the soil bearing a structure. In addition, earthquakes occur in the form of loading cycles due to sudden slips that propagate along a fault in the crust of the earth leading to the propagation of shear waves on the ground. Such stresses cause the fatigue and degradation of the soil holding the structure, if not its failure in severe cases. Consequently, characterizing the behaviour of soils and structures undergoing these types of complex loading and adapting the design methods accordingly have been an evolving research topic (O'Reilly and Brown, 1991).

While wind turbines and renewable energy have taken a vast and vital role in research lately, it is important to study the challenges encountered during the different phases of implementation, starting from the construction phase till the serviceability period. For their installation, pile jacking has become one of the techniques widely used due to its reduced noise especially in urban areas. This technique exerts quasi-static loading cycles to install a pile in the ground. These cycles could have an effect on the state of soil and its interactions with the structure. The behaviour of soils subjected to cyclic loading is an interesting research topic aimed for better design, maintenance and avoidance of collapse of structures (El Haffar et al., 2017). Despite the attempts to understand this behaviour, there are still unexplained phenomena, including cyclic mobility (Castro and Poulos, 1977), strain localization (Chiaro et al., 2013), shear band formation, and the effects of particle shape and size distribution (Tong and Wang, 2015), that are poorly modelled and thus need to be further studied in-depth.

DEM has taken a vast part of research lately, as it enables acquiring information at the grain scale. The focus of studies has been mainly on undrained cyclic deformations and liquefaction potential, (Yang et al., 2021; Martin et al., 2020; Gong et al., 2012). They studied cyclic behaviour of granular materials both before and after liquefaction and the effect of factors like the initial mean stress, void ratio, and cyclic shear amplitude. Less research has been conducted on DEM simulations of cyclic loading in drained conditions at

relatively low strain amplitude like the work of Zorzi et al. (2017) whose results showed an influence of densification and evolution of the strength of soil during cyclic loading.

To better characterize the behaviour of granular material under cyclic stress, this research aims to use discrete numerical simulations to obtain macro-micro-mechanical information on the behaviour between grains and on the possible mechanisms of energy dissipation, depending on the cyclic stress level and the sample's initial density. This is achieved by a simple cyclic drained loading path applied on an elementary volume in homogeneous conditions, implying that the material properties throughout the entire simulation domain are the same. The importance of such work lies in validating the capability of DEM to reproduce the experimental behaviour of cohesionless sand under drained triaxial monotonic and cyclic paths, that eventually enable the characterization of important soil properties.

2 DEM SIMULATIONS

In this section, DEM is used to simulate cyclic drained triaxial tests on a material that is calibrated to reproduce the behaviour of Fontainebleau NE34 sand. For this purpose, YADE, an open-source software developed by Kozicki and Donze (2009) is utilized. YADE is based on a soft-particle approach, it works in a Linux environment and is written in C++. In the next sections, the simulation properties, tests description, procedures, results and analysis will be discussed.

2.1 Inter-particle contact law

The numerical model used is a classical contact linear model with Mohr-Coulomb plasticity surface. It is characterized by constant normal and tangential stiffnesses, K_n and K_t (Figure 1) respectively, and an inter-particle friction angle φ such that :

$$\overrightarrow{F_n} = K_n \, \delta_n \, \overrightarrow{n} \qquad (1)$$

$$\Delta\overrightarrow{F_t} = -K_t \, \Delta\overrightarrow{U_t} \text{ with } \left\|\overrightarrow{F_t}\right\| \leqslant \left\|\overrightarrow{F_n}\right\| tan\varphi \qquad (2)$$

where δ_n is the overlap between spheres, $\vec{n}$ is the normal vector to the inter-particle contact plane, and $\Delta\overrightarrow{U_t}$ is the relative tangential displacement at the contact.

A rolling resistance is defined at the contact by a rolling moment M_r to model the resistance to rotation due to particle shape and angularity. It acts against the relative rotation of particles $\Delta\overrightarrow{\theta_r}$ which is controlled by a rolling stiffness K_r.

$$\Delta\overrightarrow{M_r} = -K_r \, \Delta\overrightarrow{\theta_r} \qquad (3)$$

The moment M_r has a plastic limit set by η:

$$\left\|\overrightarrow{M_r}\right\| = \left\|\overrightarrow{F_n}\right\| \eta \, min(r_A, r_B) \qquad (4)$$

where r_A and r_B are the radii of two spheres in contact.

Stiffnesses are defined from young's modulus E and the dimensionless tangential and rolling coefficients α and α_r respectively:

$$K_n = 2E\frac{r_A r_B}{r_A + r_B}; \; K_t = \alpha K_n; \; K_r = \alpha_r r_A \, r_B K_t \qquad (5)$$

In the simulations we set the values E, φ, η and α_r the same for all the particles, and therefore the stiffnesses and the rolling resistance vary from one contact to another depending on the particle size distribution.

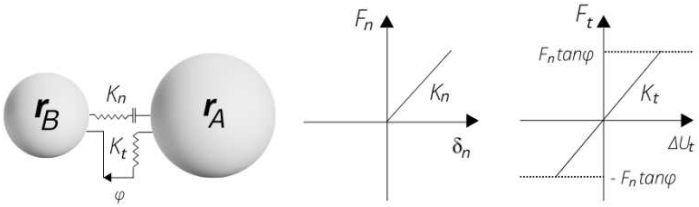

Figure 1. Contact law used in DEM simulations

2.2 Sample preparation

A cubic sample of 10,000 spherical particles with periodic boundary conditions (Radjai and Voivret, 2011) is modelled, which allows to use less particles, as well as avoid any boundary effects. The particle size distribution (PSD) of Fontainebleau NE34 is reproduced. However, representing in detail the small size tail of the distribution may yield a dramatic increase of the number of particles to be simulated, and the maximum particle size may have an effect on the optimal size of the computational domain. For this reason, the top and bottom tails of the PSD are cut (Figure 2). NE34 is a fine sub-rounded sand with a uniform distribution that varies between 0.1 mm and 0.4 mm, with a mean diameter of d_{50} = 0.21mm. The density

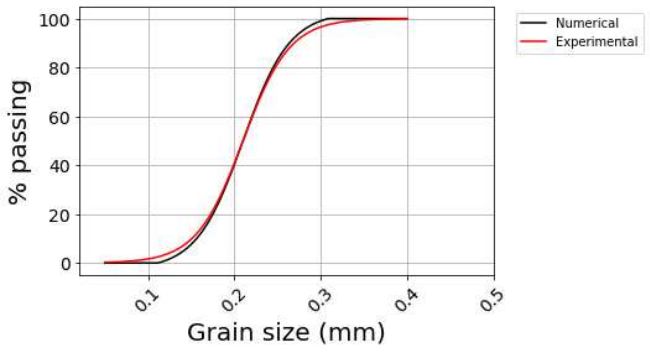

Figure 2. Expermintal and numerical particle size distribution of NE34.

of the sample is represented by the density index I_D to be consistent with the experimental results. The sample was isotropically compacted until it reaches a value of porosity initially set by I_D.

$$I_D = \frac{e_{max} - e}{e_{max} - e_{min}} \quad (6)$$

The minimum and maximum void ratios (e_{min} = *0.53* and e_{max} = 0.94) are evaluated numerically as the void ratios attained under isotropic compaction at zero and large values of φ respectively. The confining pressure (P) in all tests is set to 100 kPa during the preparation phase.

2.3 Model Calibration

Experimental data of drained monotonic triaxial tests on Fontainebleau NE34 sand are taken from Andria-Ntoanina et al. (2010) as a reference to calibrate the numerical model by varying the different parameters presented in the previous section.

Calibration is done considering drained monotonic triaxial tests at different confining pressures and densities. A drained triaxial test is simulated by imposing the stress on the lateral direction and setting it equal to the confining pressure, while controlling the strain on the axial direction by applying small strain increments. The sample is allowed to deform, thus eliminating any pressure build-up and mimicking drained conditions. The test is considered done when the strain goal is reached. Before doing so, an attempt to study the effect of each of the parameters E, φ, η and α_r is done by trial and error.

After examining the influence of each parameter on the behaviour, the various steps followed to calibrate the model are, as also mentioned by Aboul Hosn et al. (2017), the following:

• Set the value of contact stiffness modulus E and α so that it gives reasonable initial slopes of the macroscopic response at low deformations. Using the experimental value of the stiffness modulus requires high computational cost, making simulations impractical. Therefore, it is adequate to use softer particles (lower E) in a way that does not affect the overall behaviour of the simulated material.

• Calibrate η so that it fits the shear strength at large deformation.

• Vary φ set so that it reproduces the peak shear strength and thus the friction angle of the studied material.

After some trial and error, the parameters that best reproduced the behaviour of the experimental tests are the ones in Table 1. Three values of I_D are considered in the calibration of the tests to fit the experimental behaviour from the data taken from Andria-Ntoanina et al. (2010).

Table 1. Calibrated parameters of the material with experimental data.

E (MPa)	α	ϕ	α_r	η	Grain density(kg/m^3)
500	0.3	24	0.1	0.4	2650

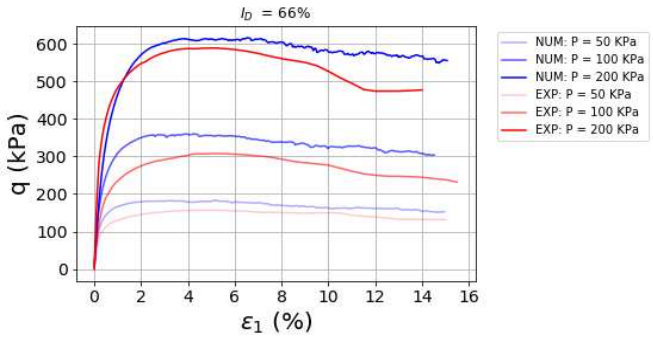

Figure 3. Deviatoric stress with axial strain by the calibration of monotonic triaxial tests with experimental data at I_D = 66% and P = 50, 100, 200 kPa.

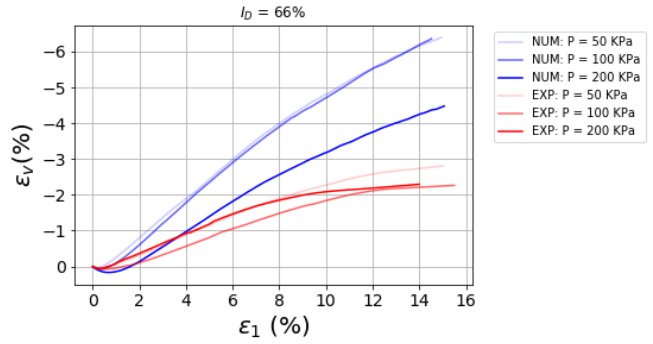

Figure 4. Volumetric strain with axial strain by the calibration of monotonic triaxial tests with experimental data at I_D = 66% and P = 50, 100, 200 kPa.

Only the case of I_D = 66% is shown in Figures 3 and 4 where three values of confining pressure are considered (P = 50, 100, 200 kPa). It can be seen from Figure 3 that even though the exact values are not attained, the overall behaviour of the deviatoric stress with axial strain at various applied pressures and density indices is captured fairly well with the used model and parameters

Looking at Figure 4, it shows that the volumetric behaviour could not be well captured, which is caused by many factors. One of them is related to the fact that the used grains are spherical instead of sub-rounded, the lack of angularity limits further compaction of the assembly as well as reduces the number of contacts per grain thus leading to a more dilatant behaviour. Another factor could be the fact that the geometries of the numerical and experimental setups are different (cubic with periodic boundary conditions in simulations while cylindrical sample with walls in experiments) leading to differences in the volumetric deformations experienced during the tests. This issue has been addressed before by Aboul Hosn et al. (2017), who showed that the volumetric behaviour is not very well reproduced with

the numerical model based on spheres, even with the introduction of a contact resistance to rolling. Therefore, it apparently constitutes a limitation of this model. We will retain the fact that the parameters chosen allow to reproduce the stress behaviour quite well.

2.4 Cyclic drained triaxial simulations

After having validated the numerical model for monotonic loading, simulations of drained cyclic triaxial tests are performed, using the same calibrated parameters (Table 1) of the contact model with rolling resistance, by stress control on the horizontal direction, while controlling strain on the axial direction which is the direction of applying the cyclic loading. The direction of loading is inversed when it reaches a limit in the deviatoric stress fixed through an initial stress ratio $\eta_0 = q_{max}/P$ where P is the confining pressure. The load is cycled around q = 0 kPa between the two extremities $-q_{max}$ and $+q_{max}$ as shown in Figure 5. The strain rate of the applied load is set such that a quasi-static regime is maintained, by keeping the inertial number much lower than the limit for quasi-static conditions, $I < 10^{-3}$ as seen with Koval et al. (2009). Tests at various cyclic stress ratios and density indices are performed to have enough data for the macroscopic and microscopic analysis afterwards. In this section, the first results from these simulations are presented.

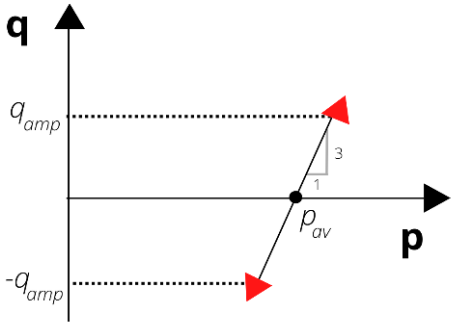

Figure 5. Stress path of the loading.

The shear modulus G and damping ratio D are two important macroscopic properties for the evaluation of many geotechnical problems and for an accurate dynamic analysis (Sitharam and Vinod, 2010). The behaviour of soil under cyclic loading is non-linear and is influenced by a variety of aspects including soil type, confining pressure, the number of loading cycles, amplitude, and rate of loading.

An attempt to evaluate both values is done where the parameters G and D are calculated at a fixed cycle (at N_{cycle} = 9) for all tests. The results are shown in Figures 6 and 7 where a comparison is done between the parameters G/G_{max} and D plotted with the deviatoric strain for different I_D. G_{max} is taken as the value of G at a very low strain amplitude. Looking at Figures 6 and 7, it can be seen that the typical evolutions of G/G_{max} and D (Seed et al., 1986) with deviatoric strain for sands are captured. Moreover, it is evident that G/G_{max} is nearly independent of the chosen density index, while frictional damping is stronger the denser the material.

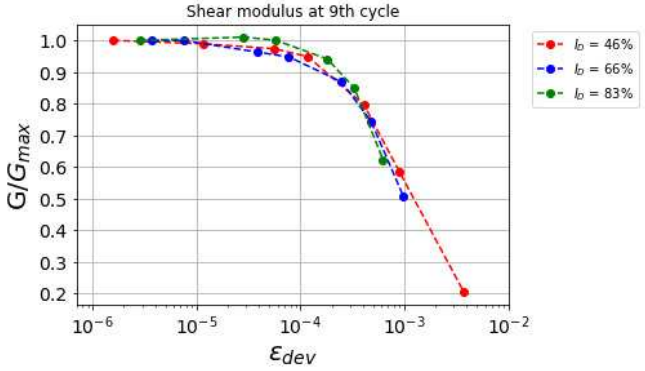

Figure 6. Modulus reduction curves with increasing deviatoric strain at I_D = 46, 66, 83 %.

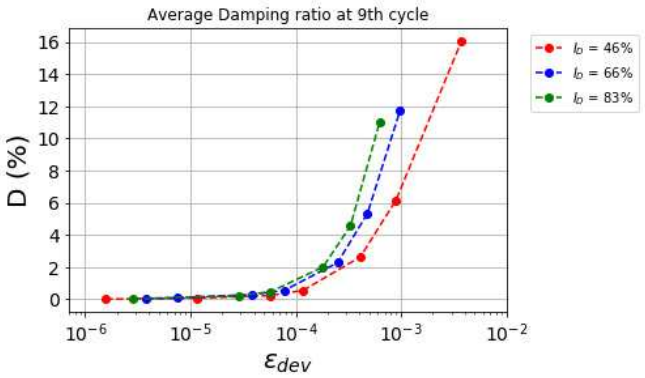

Figure 7. Damping ratio curves with increasing deviatoric strain for I_D = 46, 66, 83%.

2.5 Micromechanical analysis

To gain knowledge on the evolution of the mechanical properties of the material with the number of cycles, and to establish a relationship between the macroscopic and microscopic properties, information on the coordination number Z, the average number of contacts per particle in the sample, as well as G/G_1 and D are followed with the evolution of cycles, where G_1 is the shear modulus

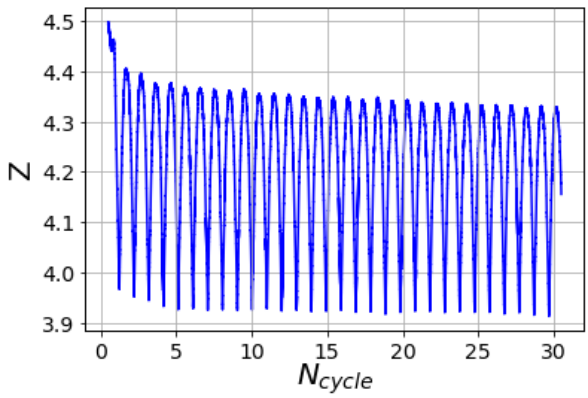

Figure 8. Variation of Z with N_{cycle} at I_D = 66%, η_0 = 0.5.

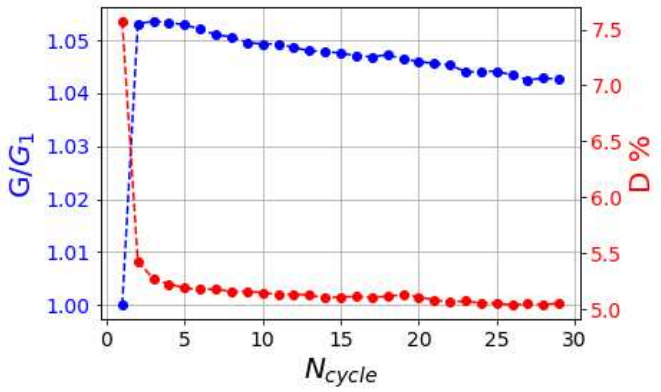

Figure 9. Variation of G/G_1 and D with N_{cycle} at I_D = 66%, η_0 = 0.5.

measured at the first cycle. The results of one of the tests is shown in Figures 8 and 9, for the case with I_D = 66%, η_0 = 0.5 and N_{cycle} = 30.

From the plots presented in Figures 8 and 9, it is clear that the first loading cycle has the highest impact on the studied parameters. A significant drop in the Z and D is observed while an increase in G/G_1 in the first loading cycle. Throughout the remaining cycles, D continues to decrease implying less energy is damped as the cycles proceed, the trend of the coordination number decreases with N_{cycle} and consequently leads to the slight decrease of G with cycles indicating that some contacts have been lost throughout cycling which might cause the decrease seen in the stiffness of the sample.

3 ACKNOWLEDGEMENTS

The authors would like to acknowledge the high performance computing center of Pays de la Loire (CCIPL) and the European project GEOLAB for their support throughout this work. The acknowledgements are extended to Gustave Eiffel University and the Region Pays de la Loire for financial support in the form of thesis grants.

4 CONCLUSIONS

The behaviour of NE34 sand is characterized numerically under cyclic loading using DEM. The particle shape effect is modelled using a rolling resistance moment. The parameters of the numerical model used are first studied and calibrated to fit the experimental behaviour of the modelled sand.

After the work done on the rolling resistance model and the calibration with experimental data on NE34 sand, it could be said that the model was able to catch the stress behaviour well while having some limitations on the volumetric behaviour. This model is then used in a series of cyclic drained triaxial tests with different density indices and cyclic stress amplitudes on the calibrated material.

A macroscopic analysis of the results follows, where the obtained curves of the modulus reduction and the damping ratio represented those of a typical sand. For comparing the macroscopic and microscopic aspects Z, G/G_1 and D are plotted with cycles. The largest variation of these parameters is observed at the first cycle, with the secant modulus increasing and the damping ratio dropping by a few percent. After the first cycle both the secant modulus and the damping ratio decrease slightly with the number of cycles. This is related to a decrease in the number of contacts.

Perspectives including further analysis of the microscopic aspect will follow, where the fabric anisotropy, the probability density function of normal forces, the orientation of strong and weak contact forces as well as friction mobilization will be studied and compared for different cases of stress amplitude and density index.

5 REFERENCES

Aboul Hosn, R., Sibille, L., Benahmed, N., & Chareyre, B. 2017. Discrete numerical modeling of loose soil with spherical particles and interparticle rolling friction, *Granular matter* **19** (1), 1–12. https://doi.org/10.1007/s10035-016-0687-0

Andria-Ntoanina, I., Canou, J., & Dupla, J.-C. 2010. Caractérisation mécanique du sable de Fontainebleau NE34 à l'appareil triaxial sous cisaillement monotone. *Rapport projet SOLCYP*. 21p.

Castro G., & Poulos S. J. 1977. Factors affecting liquefaction and cyclic mobility. Journal of the Geotechnical Engineering Division, **103**(6), 501-516. https://doi.org/10.1061/AJGEB6.0000433

Chareyre B., Villard P. 2005. Dynamic spar elements and discrete element methods in two dimensions for the modeling of soil-inclusion problem), *Journal of Engineering Mechanics* **131**, 689–698. https://doi.org/10.1061/(ASCE)0733-9399(2005)131:7(689)

Chiaro, G., Kiyota, T., & Koseki, J. 2013. Strain localization characteristics of loose saturated Toyoura sand in undrained cyclic torsional shear tests with initial static shear. *Soils and Foundations*, **53**(1), 23-34. https://doi.org/10.1016/j.sandf.2012.07.016

Cundall, P. A., & Strack, O. D. 1979. A discrete numerical model for granular assemblies, *Géotechnique* **29** (1), 47–65. https://doi.org/10.1680/geot.1979.29.1.47

Di Prisco, C. G., & Wood, D. M. 2012. *Mechanical behaviour of soils under environmentallly induced cyclic loads* (Vol. 534), Springer Science & Business Media, Berlin/Heidelberg, Germany.

El Haffar, I., Blanc, M., & Thorel, L. 2017. Impact of pile installation method on the axial capacity in sand, *Géotechnique Letters* **7** (3), 260–265. https://doi.org/10.1680/jgele.17.00036

Gong, G., Thornton, C., & Chan, A. H. 2012. DEM simulations of undrained triaxial behavior of granular material, *Journal of engineering mechanics* **138** (6), 560–566. https://doi.org/10.1061/(ASCE)EM.1943-7889.0000366

Koval, G., Roux, J.-N., Corfdir, A., & Chevoir, F. 2009. Annular shear of cohesionless granular materials: From the inertial to quasistatic regime, *Physical Review E* **79** (2), 021306. https://doi.org/10.1103/PhysRevE.79.021306

Kozicki, J., & Donze, F. V. 2009. YADE-OPEN DEM: An open-source software using a discrete element method to simulate granular material, *Engineering Computations* **26** (7), 786-805. https://doi.org/10.1108/02644400910985170

Martin, E. L., Thornton, C., & Utili, S. 2020. Micromechanical investigation of liquefaction of granular media by cyclic 3D DEM tests, *Géotechnique* **70** (10), 906–915. https://doi.org/10.1680/jgeot.18.P.267

O'Reilly, M. P., & Brown, S. F. (Eds.). 1991. *Cyclic loading of soils: from theory to design*, Blackie, London, UK.

Radjai F., Voivret C. 2011. Periodic boundary conditions. Radjai F., Dubois F. *Discrete-element modeling of granular materials*, Wiley-Iste, Hoboken, New Jersey, USA.

Seed, H. B., Wong, R. T., Idriss, I. M., & Tokimatsu, K. 1986. Moduli and damping factors for dynamic analyses of cohesionless soils, *Journal of geotechnical engineering* **112**(11), 1016-1032. https://doi.org/10.1061/(ASCE)07339410(1986)112:11(1016)

Sitharam, T. G., & Vinod, J. S. 2010. Evaluation of shear modulus and damping ratio of granular materials using discrete element approach, *Geotechnical and Geological Engineering* **28**(5), 591-601. http://dx.doi.org/10.1007/s10706-010-9317-5

Tong, L., & Wang, Y. H. 2015. DEM simulations of shear modulus and damping ratio of sand with emphasis on the effects of particle number, particle shape, and aging. *Acta Geotechnica*, **10**, 117-130. https://hdl.handle.net/1783.1/65633

Yang, M., Taiebat, M., Mutabaruka, P., & Radjaï, F. 2021. Evolution of granular materials underisochoric cyclic simple shearing, *Physical Review E* **103**(3), 032904. https://doi.org/10.1103/PhysRevE.103.032904

Zorzi, G., Kirsch, F., Gabrieli, F., & Rackwitz, F. 2017. Long-term cyclic triaxial tests with DEM simulations. *PARTICLES V: proceedings of the V International Conference on Particle-Based Methods: fundamentals and applications* (Eds: Wriggers P., Bischoff M., Oñate E., Owen D.R.J. and Zohdi T.), 273–284. CIMNE, Barcelona, Spain. http://hdl.handle.net/2117/187133